JBC RESEARCH ARTICLE

Discovery of an L-amino acid ligase implicated in *Staphylococcal* sulfur amino acid metabolism

Received for publication, May 31, 2022, and in revised form, August 10, 2022 Published, Papers in Press, August 19, 2022,
https://doi.org/10.1016/j.jbc.2022.102392

Jordan L. Pederick[1], Aimee J. Horsfall[2,3], Blagojce Jovcevski[4,5], Jack Klose[4], Andrew D. Abell[2,3], Tara L. Pukala[4], and John B. Bruning[1,*]

From the [1]Institute for Photonics and Advanced Sensing (IPAS), School of Biological Sciences, and [2]Institute for Photonics and Advanced Sensing (IPAS), School of Physical Sciences, The University of Adelaide, Adelaide, South Australia, Australia; [3]ARC Centre of Excellence for Nanoscale BioPhotonics (CNBP), Adelaide, South Australia, Australia; [4]Department of Chemistry, and [5]School of Agriculture, Food and Wine, The University of Adelaide, Adelaide, South Australia, Australia

Edited by Karen Fleming

Enzymes involved in *Staphylococcus aureus* amino acid metabolism have recently gained traction as promising targets for the development of new antibiotics, however, not all aspects of this process are understood. The ATP-grasp superfamily includes enzymes that predominantly catalyze the ATP-dependent ligation of various carboxylate and amine substrates. One subset, L-amino acid ligases (LALs), primarily catalyze the formation of dipeptide products in Gram-positive bacteria, however, their involvement in *S. aureus* amino acid metabolism has not been investigated. Here, we present the characterization of the putative ATP-grasp enzyme (SAOUHSC_02373) from *S. aureus* NCTC 8325 and its identification as a novel LAL. First, we interrogated the activity of SAOUHSC_02373 against a panel of L-amino acid substrates. As a result, we identified SAOUHSC_02373 as an LAL with high selectivity for L-aspartate and L-methionine substrates, specifically forming an L-aspartyl–L-methionine dipeptide. Thus, we propose that SAOUHSC_02373 be assigned as L-aspartate–L-methionine ligase (LdmS). To further understand this unique activity, we investigated the mechanism of LdmS by X-ray crystallography, molecular modeling, and site-directed mutagenesis. Our results suggest that LdmS shares a similar mechanism to other ATP-grasp enzymes but possesses a distinctive active site architecture that confers selectivity for the L-Asp and L-Met substrates. Phylogenetic analysis revealed LdmS homologs are highly conserved in *Staphylococcus* and closely related Gram-positive Firmicutes. Subsequent genetic analysis upstream of the *ldmS* operon revealed several *trans*-acting regulatory elements associated with control of Met and Cys metabolism. Together, these findings support a role for LdmS in *Staphylococcal* sulfur amino acid metabolism.

Staphylococci are Gram-positive bacteria that are both commensal and major human pathogens. *Staphylococcus aureus* remains a threat in both hospital and community settings being responsible for infections ranging in severity from mild to life-threatening, with the latter likely numbering in the hundreds of thousands to millions per year worldwide (1, 2). Furthermore, the ability of *S. aureus* to develop antibiotic resistance is of major concern. While antibiotics have traditionally targeted essential bacterial processes, increasing resistance of human pathogenic bacteria to current antibiotics has led to the investigation of new targets for combating infection. One avenue being explored is the characterization of nonessential metabolic pathways to identify and understand roles in virulence and persistence. In *S. aureus*, there is mounting evidence that nonessential aspects of amino acid metabolism, particularly those involving Met and Cys metabolism, become conditionally essential in a host environment and therefore present as new targets for the development of antibiotics and antibiotic adjuvants (3–7). Importantly, to fully exploit such targets, a full understanding of these metabolic pathways is key.

In bacteria, numerous enzymes of the ATP-grasp superfamily are known to catalyze the ATP-dependent formation of a wide range of molecular products (8, 9). While functionally distinct ATP-grasp ligases possess low amino acid sequence identity (commonly <20%), these enzymes share a similar global structure, which is defined by a conserved ATP-binding site termed the ATP-grasp fold. A member of this superfamily, L-amino acid ligases (LALs), produce a range of L-amino acid dipeptide or oligopeptide products with quite strict substrate specificities. To date, 14 such LALs have been characterized with 12 catalyzing dipeptide formation and two forming oligopeptide products, many of which contain nonstandard amino acids and possess antibiotic properties (Table S1). Structural and kinetic characterization of the LAL L-Ala–L-anticapsin ligase (BacD), which produces the antibiotic dipeptide L-Ala–L-anticapsin (Bacilysin), supports LALs sharing the same general mechanism as other ATP-grasp enzymes (Fig. 1). This step-wise mechanism involves the ligation of a carboxylate substrate and an amine substrate, proceeding through the formation of two phosphorylated intermediates. The first step of the reaction involves formation of an enzyme-ATP·Mg^{2+} complex. Following this, the carboxylate substrate binds to this complex and the γ-phosphate undergoes nucleophilic attack to form an acylphosphate

* For correspondence: John B. Bruning, john.bruning@adelaide.edu.au.

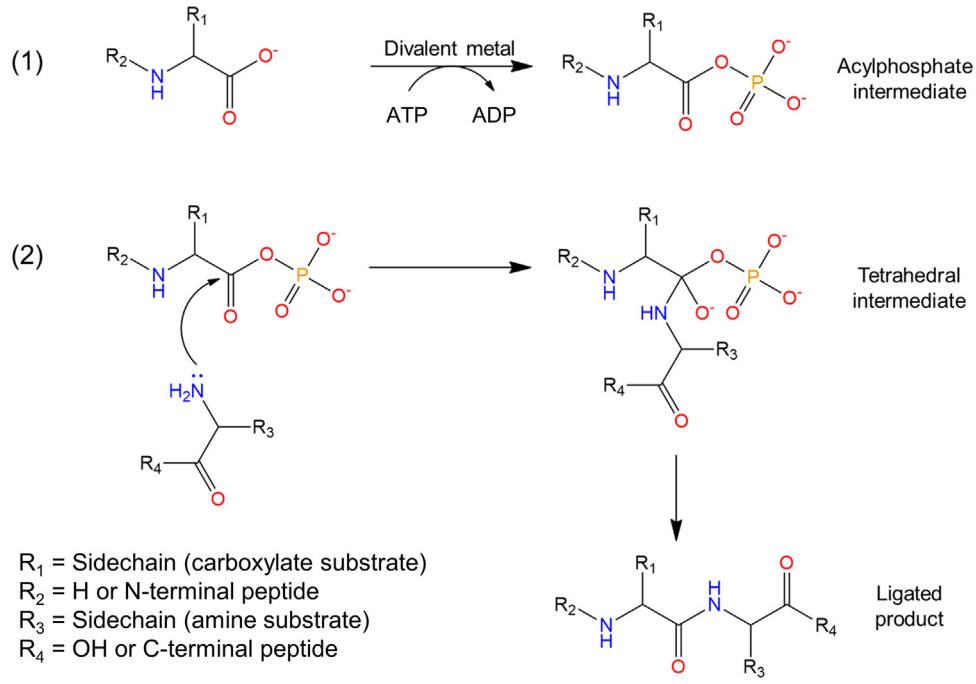

Figure 1. General reaction scheme of ATP-grasp enzymes catalyzing the formation of peptide products.

intermediate. Next, the amine substrate, which must be deprotonated, attacks the carbonyl group of the acylphosphate intermediate to form a phosphorylated tetrahedral intermediate. This deprotonation step is considered to be mediated by an active site base, however, for many ATP-grasp enzymes, the mechanism of this deprotonation step remains unclear (9). Finally, this tetrahedral intermediate collapses to give the ligated product. The investigation of LALs has focused on exploiting their catalytic properties for synthetic applications. As a result, the existence and functional roles of LALs in human-pathogenic species such as *S. aureus* has yet to be investigated in detail. Given the peptide-forming activity of LALs, we suspected that this avenue of investigation may provide insight into unique aspects of amino acid metabolism.

In our search for candidate LALs, we discovered a putative ATP-grasp enzyme of *S. aureus* NCTC 8325 encoded by *saouhsc_02373*. While the activity or physiological role of SAOUHSC_02373 was unknown, high-throughput transposon mutagenesis of *S. aureus* NCTC 8325 identified the target gene as nonessential in rich growth media (10, 11). Aligning the amino acid sequence of SAOUHSC_02373 against that of characterized ATP-grasp enzymes, including LALs, revealed low sequence identity, indicative of a new substrate preference and catalytic activity (Table S2). Although confident assignment of SAOUHSC_02373 as an LAL was not possible from amino acid sequence alone, the genetic localization of SAOUHSC_02373 suggested it may possess LAL activity. The operon containing *saouhsc_02373* contains two genes, with *saouhsc_02373* being positioned downstream of *hmrA*, which encodes a M20D family metallopeptidase. Interestingly, in addition to being identified as a methicillin resistance factor, recent characterization of *S. aureus* HmrA revealed carboxypeptidase activity against a range of peptide substrates but displays a preference for hydrolysis of L-Met–L-X dipeptides, an activity shared by other M20D family carboxypeptidases (12, 13). While the physiological role of HmrA remains unclear, it has been speculated to participate in Met recycling and acquisition, as other Gram-positive species encode *hmrA* homologs in operons containing Met transporters (14). This localization with *hmrA* suggested that SAOUHSC_02373 may therefore be an LAL involved in *S. aureus* sulfur amino acid metabolism, warranting further investigation.

Here, we present the first reported characterization of SAOUHSC_02373 from *S. aureus* NCTC 8325. The substrate specificity of SAOUHSC_02373 was probed by screening against the 20 common L-amino acids as substrates, confirming LAL activity and identifying a preference for L-Met and L-Asp as substrates. Further screening against a panel of related substrate analogs yielded no improvements in activity, supporting L-Met and L-Asp as the preferred substrates of SAOUHSC_02373. Characterization of the reaction product by mass spectrometry (MS) and NMR spectroscopy revealed that SAOUHSC_023773 catalyzes the synthesis of the heteropeptide product L-Asp–L-Met. To our knowledge, this is the first report of an LAL preferentially accepting L-Asp as the carboxylate substrate. We therefore propose to assign SAOUHSC_02373 as L-aspartate–L-methionine ligase or LdmS. The structure of LdmS was determined by X-ray crystallography revealing distinct conformational states, suggestive of structural rearrangement during catalysis. By using a combination of molecular docking and site-directed mutagenesis, the determinants of selectivity for the L-Asp and L-Met substrates were identified, with distinct polar and hydrophobic cavities accepting the respective substrates. These results support LdmS sharing the same general mechanism reported

for other enzymes of the ATP-grasp superfamily. To gain insight into the physiological role of LdmS, phylogenetic analysis was performed to identify the distribution of LdmS homologs throughout Prokaryota. This revealed high conservation of LdmS within the Gram-positive Firmicutes genera *Staphylococcus*, *Mammaliicoccus*, *Macrococcus*, and *Abyssicoccus*. Furthermore, genetic analysis upstream of the *hmrA/ldmS* operon identified the presence of consensus sequences for several *trans*-acting elements involved in the transcriptional repression of genes participating in sulfur amino acid metabolism. Together, this supports a role for LdmS in *Staphylococcal* sulfur amino acid metabolism.

Results

Identification of SAOUHSC_02373 as L-*aspartate–*L-*methionine ligase*

First, a colorimetric assay of phosphate was used to determine if SAOUHSC_02373 possessed LAL activity (15, 16). Initially, activity was measured for a reaction containing all 20 standard L-amino acids as substrates (Fig. 2*A*). A strong signal was observed, with no phosphate release detected in the ATP only and no-enzyme control reactions, providing strong evidence that SAOUHSC_02373 possesses LAL activity. Due to the preference of HmrA for accepting L-Met–L-X dipeptides as substrates, the experiment was repeated with L-Met omitted, resulting in a large reduction of LAL activity. Given this apparent preference for L-Met as a substrate, the activity of SAOUHSC_02373 was next screened for all combinations of the 20 standard amino acids with L-Met as a constant substrate (Fig. 2*B*). Activity was only detected for L-Met + L-Asp and L-Met + L-Asn substrate pairs, with the latter displaying 50-fold lower activity. Given the preference observed for L-Met + L-Asp, the experiment was then repeated for all combinations with L-Asp as a constant substrate. This revealed that other hydrophobic amino acids including L-Phe, L-Val, L-Leu, and L-Ile may substitute for L-Met, however, the L-Met + L-Asp substrate pair was strongly favored, with ~10-fold higher activity than all other substrate combinations assayed. Additionally, no activity was detected with either L-Met or L-Asp as the lone substrate, suggesting that substrate recognition by SAOUHSC_02373 is mediated by two chemically distinct binding sites.

A series of L-Met and L-Asp analogs was screened to further probe the substrate selectivity of SAOUHSC_02373 (Table 1). First, the stereoselectivity of SAOUHSC_02373 was probed with D-Met and D-Asp as substrates. Neither were accepted when paired with the corresponding L-stereoisomer, indicating that SAOUHSC_02373 is stereoselective for L-amino acid substrates. Modification of the L-Met scaffold was tolerated but largely resulted in reduced activity. While L-Met could be effectively replaced by seleno-DL-Met, the shorter and more polar L-homoCys or the bulkier L-Met sulfoxide, L-Met sulfoximine, and o-acetyl-L-Ser showed reduced activity, suggesting that the length and hydrophobic nature of L-Met is most effectively accommodated. In contrast, L-homoSer could not replace L-Met as a substrate. Formylation or acetylation of the L-Met amino group resulted in greatly reduced or no activity. Modification of the L-Met carboxylate group was better tolerated, with L-Met methyl ester producing ~1/3 the activity observed for L-Met, while the bulkier carboxylate modification of L-Met–Gly was not accepted. In contrast to L-Met, alteration of the L-Asp scaffold resulted in loss of activity in nearly all cases, with L-Asn the only exception. Analogs with modified

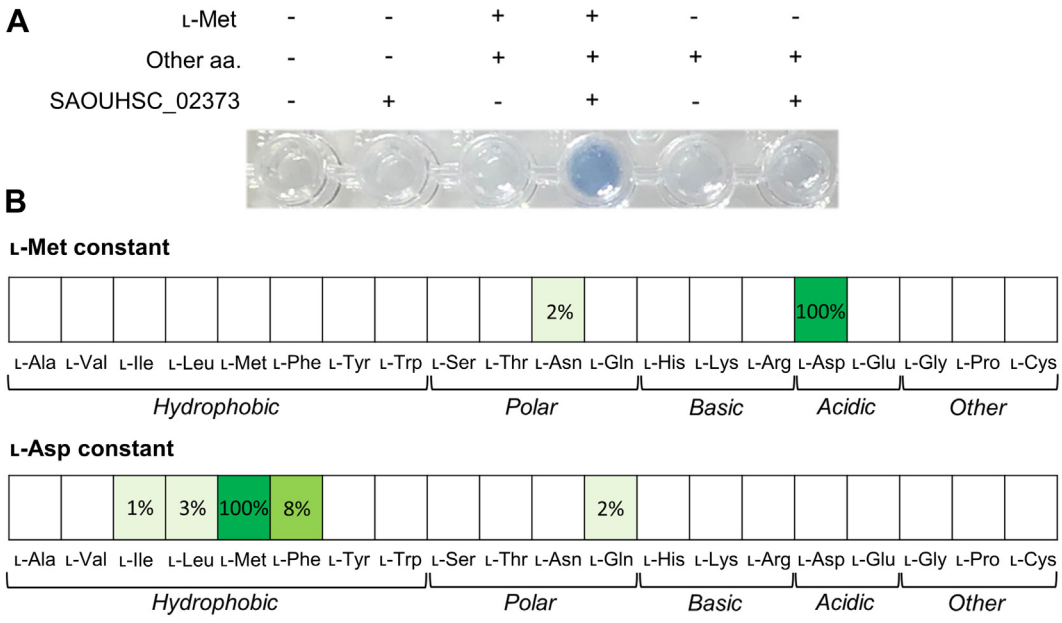

Figure 2. Screening of L-amino acid substrates reveals a preference for L-Met and L-Asp. *A*, probing LAL activity of SAOUHSC_02373. "Other aa." refers to the 19 common amino acids excluding L-Met. Reactions contained 50 mM Tris–HCl pH 8.0, 5 mM $MgCl_2$, 500 μM ATP, 50 nM LdmS, and 2 mM of each included L-amino acid substrate. *B*, identification of L-amino acid substrates utilized by SAOUHSC_02373. Activity is reported relative to the L-Met + L-Asp substrate pair and indicated by green shading, with no shading indicating no measurable activity. Activity for the L-Asp + L-Met substrate pair was 2.99 μmol s^{-1} mg^{-1} SAOUHSC_02373. Reactions contained 50 mM Tris–HCl pH 8.0, 5 mM $MgCl_2$, 500 μM ATP, 50 nM LdmS, and 5 mM of each L-amino acid substrate. All experiments were performed at least twice. LAL, L-amino acid ligase; LdmS, L-aspartate–L-methionine ligase.

Table 1
Screening of L-Met and L-Asp analogs reveals substrate preference of SAOUHSC_02373

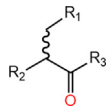

Substrate analogs[a]	R_1	R_2	R_3	Activity (%)[b]
L-Met analogs[c]				
D-Met	CH_2SCH_3	NH_3^+	O^-	0
seleno-DL-Met[d]	CH_2SeCH_3	NH_3^+	O^-	90 ± 14
L-homoCys	CH_2SH	NH_3^+	O^-	40 ± 5
L-homoSer	CH_2OH	NH_3^+	O^-	0
L-Met sulfoxide	$CH_2S(O)CH_3$	NH_3^+	O^-	25 ± 2
L-Met sulfoximine	$CH_2S(ONH)CH_3$	NH_3^+	O^-	4.6 ± 0.5
o-acetyl-L-Ser	$OCOCH_3$	NH_3^+	O^-	2.0 ± 0.3
N-formyl-L-Met	CH_2SCH_3	NHCHO	O^-	2.4 ± 0.1
N-acetyl-L-Met	CH_2SCH_3	$NHCOCH_3$	O^-	0
L-Met methyl ester	CH_2SCH_3	NH_3^+	OCH_3	35 ± 1
L-Met–Gly	CH_2SCH_3	NH_3^+	$NHCH_3COO^-$	0
L-Asp analogs[e]				
D-Asp	COO^-	NH_3^+	O^-	0
L-Asn	$CONH_2$	NH_3^+	O^-	2.0 ± 0.1
DL-Asp β-methyl ester[d]	$COOCH_3$	NH_3^+	O^-	0
L-homoSer	CH_2OH	NH_3^+	O^-	0
o-acetyl-L-Ser	$OCOCH_3$	NH_3^+	O^-	0
L-Glu	CH_2COO^-	NH_3^+	O^-	0
L-malate	COO^-	OH	O^-	0
N-carbamoyl-DL-Asp[d]	COO^-	$NHCONH_2$	O^-	0.9 ± 0.1
Gly–L-Asp	COO^-	$NHCOCH_2NH_3^+$	O^-	0
L-Asp–Gly	NH_3^+	COO^-	$NHCH_2COO^-$	0

[a] Stereochemistry is indicated for each assayed analog. Waved line in scaffold indicates the screened analog may be the D- or L-stereoisomer or a racemic mixture of both.
[b] Activity relative to L-Met + L-Asp substrate pair. Error represents SD of two experiments with two technical replicates. Reactions contained 50 mM Tris–HCl pH 8.0, 5 mM $MgCl_2$, 500 μM ATP, 5 mM of each L-amino acid or analog being assayed, and 5 nM or 50 nM LdmS.
[c] Assayed in the presence of L-Asp.
[d] Racemic mixture of D- and L-stereoisomers.
[e] Assayed in the presence of L-Met.

sidechain functionalities including the smaller L-homoSer and bulkier DL-Asp β-methyl ester, L-Glu, and o-acetyl-L-Ser showed no detectable activity, suggesting SAOUHSC_02373 has evolved to specifically recognize the β-carboxylate sidechain of L-Asp. Furthermore, modifications of the L-Asp amino and α-carboxylate groups were poorly accommodated, with L-malate, Gly–L-Asp, and L-Asp–Gly inactive, while N-carbamoyl-DL-Asp displayed 100-fold lower activity than with L-Asp. Together, this analysis supports that L-Met and L-Asp are the substrate pair most effectively recognized by SAOUHSC_02373.

With L-Met and L-Asp identified as the preferred substrates of SAOUHSC_02373, the identity of the reaction product was subsequently investigated. Analysis of a reaction containing L-Asp and L-Met by electrospray ionization (ESI+)-MS revealed predominant peaks at 265.08 and 287.06 *m/z*, corresponding to a hetero-dipeptide (and the sodiated adduct) consisting of L-Met and L-Asp, with no ions corresponding to either homo-dipeptide or larger oligomers observed (Fig. 3*A*). To determine the connectivity of the hetero-dipeptide product, the 265.08 *m/z* ion was interrogated by MS/MS analysis and the resulting fragmentation pattern compared to that collected for L-Met–L-Asp and L-Asp–L-Met dipeptide standards (Fig. 3*B*). The fragmentation pattern of the hetero-dipeptide product closely resembled that of the L-Asp–L-Met standard, supporting that SAOUHSC_02373 catalyzes the formation of L-Asp–L-Met and not L-Met–L-Asp. To supplement this, the product of a separate reaction containing the L-Met + L-Asp substrate pair was isolated by RP-HPLC and characterized by 1D and 2D NMR spectroscopy, with the resulting spectra supporting the assignment of the isolated product as L-Asp–L-Met (Figs. S1 and S2). Notably, this identifies SAOUHSC_02373 as a dipeptide forming LAL and the first reported LAL to preferentially accept L-Asp as the carboxylate substrate.

Having identified the L-Asp–L-Met dipeptide forming activity of SAOUHSC_02373, the effects of varying parameters including nucleoside triphosphate, divalent metals, and pH were investigated (Fig. S3). The results matched those of other ATP-grasp enzymes, with SAOUHSC_02373 having a strict requirement for ATP and a divalent metal, preferably Mg^{2+}, and showing optimal activity between pH 7.5 and 8.5 (9). The kinetic parameters of SAOUHSC_02373 were also measured for ATP, L-Met, and L-Asp (Fig. 4). The K_M for ATP and k_{cat} were determined as 310 ± 20 μM and 48 ± 1 s^{-1}. This is consistent with other members of the ATP-grasp superfamily, which generally possess a K_M for ATP in the micromolar range. A substantial difference was observed between the K_M values of the amino acid substrates, being 11,000 ± 600 μM and 580 ± 20 μM for L-Asp and L-Met, respectively. Despite the seemingly low affinity of SAOUHSC_02373 for L-Asp, we predict that this is representative of high substrate abundance under physiological conditions, as L-Asp is one of the most abundant cytoplasmic amino acids in *S. aureus* (17–19). While most L-Asp utilizing enzymes of *S. aureus* have not been characterized, a recent investigation of L-Asp transcarbamoylase determined the L-Asp K_M as 4.5 mM (20). In multiple other bacterial species, L-Asp–utilizing enzymes such

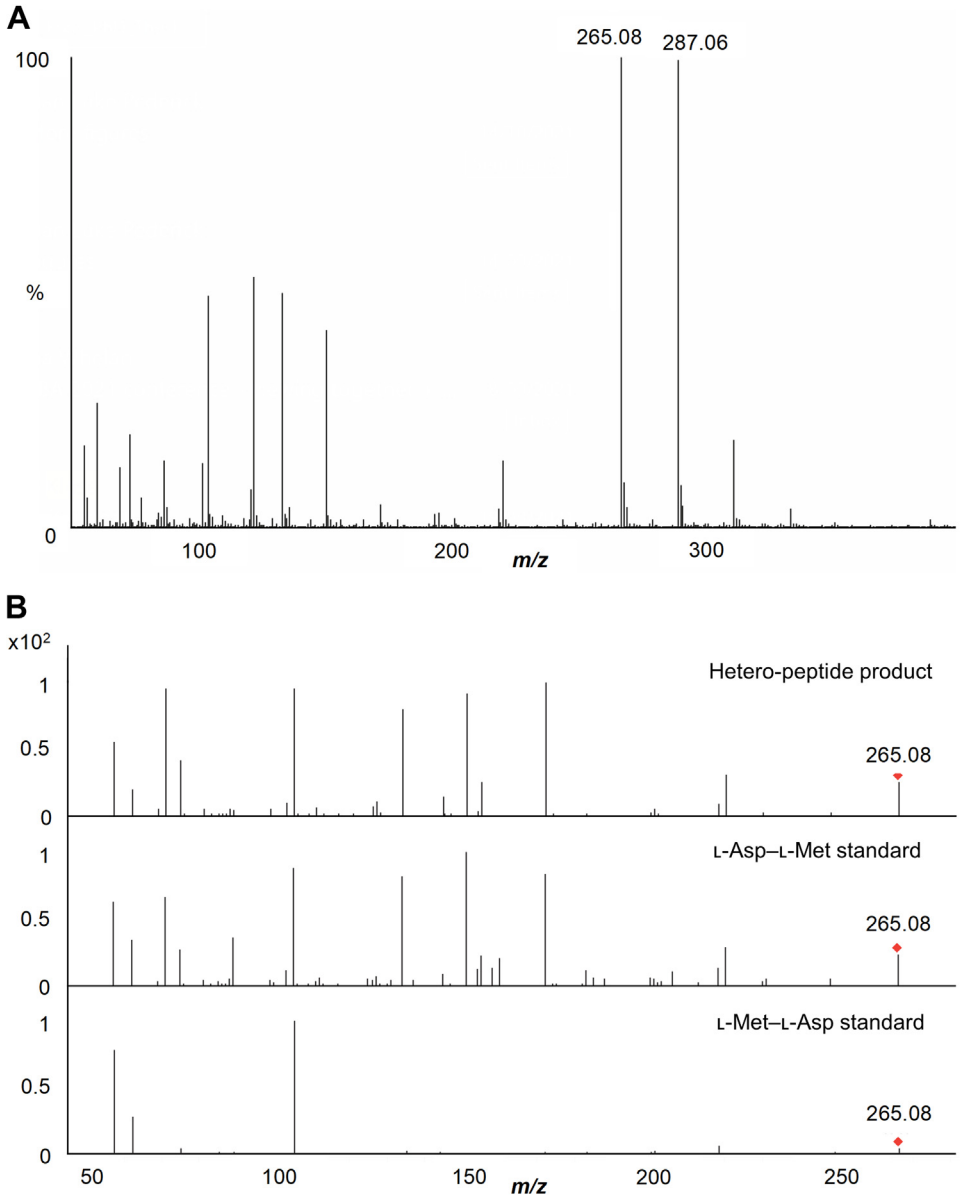

Figure 3. Identification of the hetero-peptide product by MS. *A*, ESI-TOF spectrum for LdmS reaction with L-Met and L-Asp as substrates. The predominant peaks at 265.08 and 287.06 *m/z* correspond to a hetero-peptide of L-Met and L-Asp in the form of protonated and sodiated adducts, respectively. *B*, MS/MS analysis of the 265.08 *m/z* hetero-peptide product. The fragmentation pattern matches that of L-Asp–L-Met, with major ions present in both spectra. ESI, electronspray ionization; LdmS, L-aspartate–L-methionine ligase; MS, mass spectrometry.

as aspartokinase I–III have also been reported to possess similar K_M values for L-Asp, ranging between 1.9 and 21 mM (21–25). Investigations of Met limitation for *S. aureus* have also revealed that mutant strains with an inactivated *de novo* Met biosynthesis pathway require up to 100 μM L-Met for a normal growth phenotype (5). While information regarding exact metabolite concentrations in *S. aureus* is not yet available, these observations support that both L-Asp and L-Met are likely to be present at sufficient concentrations in *S. aureus* to support the formation of the L-Asp–L-Met product under physiological conditions. Considering this, and the clear preference toward L-Asp and L-Met as substrates, we propose that SAOUHSC_02373 be assigned as L-aspartate–L-methionine ligase, herein referred to as LdmS.

Structural characterization of LdmS

The structure of LdmS was characterized by X-ray crystallography in order to understand the determinants of substrate selectivity. This resulted in the capture of two high resolution structures in distinct conformational states: an open form (1.37 Å), complexed with ADP, Mg^{2+}, and Na^{+}, and a closed form (2.00 Å), with citrate from the crystallization buffer binding adjacent to ADP. The overall fold of LdmS was comparable to that of other ATP-grasp enzymes, which are generally composed of three or four domains. LdmS adopted the latter architecture, consisting of Domains N (Res. 1–125), A (Res. 126–219), B (Res. 220–318), and C (Res. 319–397), with the catalytic center positioned at their interface (Fig. 5). Domains A and B form the ATP-grasp fold,

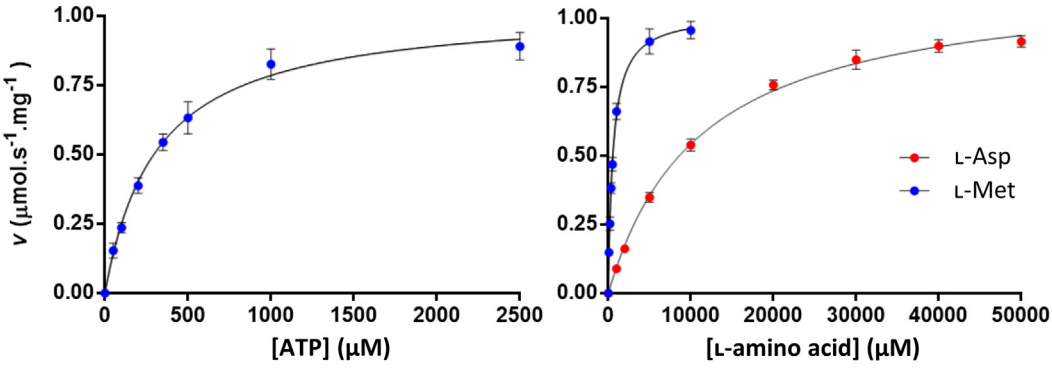

K_M ATP (µM)	K_M L-Asp (µM)	K_M L-Met (µM)	K_{cat} (s^{-1})
310 ± 20	11 000 ± 600	580 ± 20	48 ± 1

Figure 4. Determination of kinetic parameters for LdmS with ATP, L-Asp, and L-Met substrates. Reactions contained 50 mM Tris–HCl pH 8.0, 100 mM KCl, 5 mM $MgCl_2$, 1 mM phosphoenolpyruvate, 400 µM NADH, 6 to 10 U ml^{-1} pyruvate kinase, 9 to 14 U·ml^{-1} lactate dehydrogenase, 25 nM LdmS, and varying concentrations of ATP, L-Asp, and L-Met. For determination of K_M values, two of the three substrates ATP, L-Asp, and L-Met were present at fixed concentrations of 2.5 mM, 50 mM, and 10 mM, respectively, being at least 5× the measured K_M value for each substrate. The varied substrate was assayed at seven concentrations ranging between at least 0.2× and 5× the measured K_M. All data is presented as the mean ± SD, n = 3 experiments, each with two technical replicates. LdmS, L-aspartate–L-methionine ligase.

with the substrate-binding pocket formed by contributions from all four domains. Both crystal structures were indicative of LdmS being a monomer, with no oligomeric interfaces present. This was supported by native MS analysis which revealed LdmS is predominantly monomeric in solution (Fig. S4). Comparison of the open and closed forms revealed distinct conformational changes when the active center was fully occupied. In the open form, disorder is observed for two large loop regions, the P-loop (Res. 175–186) and an *N*-terminal loop region, herein referred to as the N-loop (Res. 28–38). These loops become ordered in the closed form. The P-loop is observed to adopt the typical conformation observed for ATP-grasp enzymes, stacking over the interface between the phosphates of ADP and bound citrate, with Res. 204 to 209 stabilizing the P-loop through several hydrogen bond interactions. Finally, the N-loop closes over the P-loop, fully enclosing the active site.

Structure of LdmS in complex with ADP, citrate, Mg^{2+}, and Na^+

The closed form of LdmS provides a complete snapshot of the substrate-binding cavity. The characteristic binding mode of the nucleoside substrate within the ATP-grasp fold is conserved for LdmS (Fig. 6*A*). The adenine group of ADP is positioned in a hydrophobic pocket being sandwiched between Val171, Val186, Ile188, Leu290, Ile300, and Lys217 and is further stabilized through hydrogen bonds involving the sidechains of Lys173 and Glu215 and the mainchain backbone of Gln216 and Ile218. An additional hydrogen bond between Tyr190 of domain A and the backbone amide of Lys248 appears to facilitate closure of the loop region between β10 and β11 (Res. 246–252) over the bound ADP. The ADP ribose is stabilized by several hydrogen bonds involving the sidechain of Thr246 and two ordered solvent molecules, W_A and W_B. The sidechain and backbone of Thr246 also

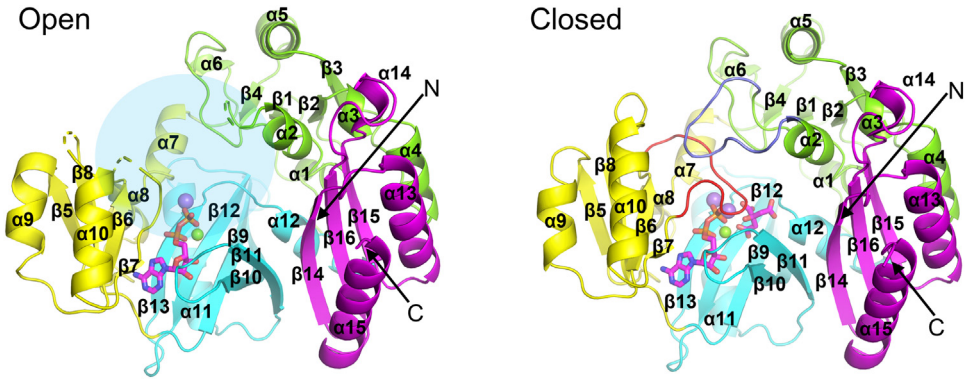

Figure 5. The overall structure of LdmS. *Left*, the open form of LdmS (PDB: 7R8P) in complex with Mg·ADP and Na^+. The P-loop and N-loop are disordered (*blue shading*). *Right*, the closed form of LdmS (PDB: 7R8Q) in complex with Mg·ADP, Na^+, and citrate. The presence of the organic acid resulted in stabilization of the P-loop (*red*) and N-loop (*purple*) to form a distinct cavity. Domains N, A, B, and C are shown as *green*, *yellow*, *cyan*, and *magenta cartoon*, respectively. ADP and citrate are shown as *pink sticks*. Bound Mg^{2+} and Na^+ are shown as *green* and *purple spheres*, respectively. LdmS, L-aspartate–L-methionine ligase.

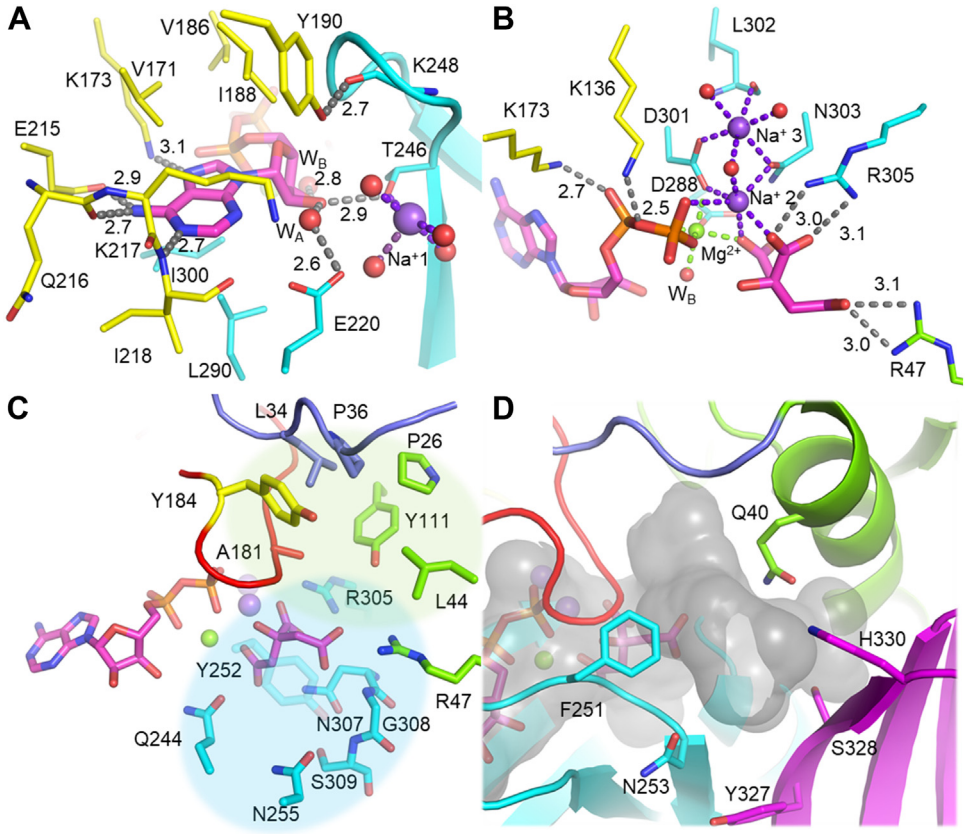

Figure 6. The closed form of LdmS reveals active site architecture. *A*, recognition of the adenosine group of ADP. *B*, metal coordination network involving phosphates and citrate. *C*, the polar cavity (*blue shading*) and hydrophobic cavity (*green shading*) present within the LdmS active site. *D*, surface representation of the substrate-binding pocket and the solvent accessible entry/exit point. Domains N, A, B, and C are shown as *green*, *yellow*, *cyan*, and *pink cartoons*, with interacting residues shown as *sticks*. Bound ADP and citrate are shown as *pink sticks*. Na^+ and Mg^{2+} and solvent are shown as *purple*, *green*, and *red spheres* respectively, with the metal coordination spheres indicated by *colored dashes*. Hydrogen bond interactions are represented by *gray dashes*, with distances labeled in angstroms. LdmS, L-aspartate–L-methionine ligase.

coordinate a Na^+ ion (Na^+ 1), however, this does not interact directly with ADP and is likely present due to high Na^+ content (>1 M) of the crystallization buffer. The ADP α and β phosphates are stabilized through ionic interactions with Lys136 and Lys173 and the backbone amide of Gly183 (Fig. 6*B*). In enzymes of the ATP-grasp superfamily, ATP is coordinated by two divalent metals, generally Mg^{2+}, which facilitate transfer of the γ phosphate to the carboxylate substrate. For LdmS, one Mg^{2+} was preserved, while the second Mg^{2+} was replaced by Na^+ 2. The bound Mg^{2+} coordinates both the α and β phosphates and the sidechains of Asp288 and Asp301, with W_B and bound citrate completing the coordination sphere. Ordinarily, the second Mg^{2+} would bridge between the β and γ phosphate following phosphoryl transfer to the carboxylate substrate. Instead, Na^+ 2 substitutes this role and bridges the β-phosphate and bound citrate. Citrate is stabilized by a pair of ionic interactions involving Arg47 and Arg305, occupying the expected position of the γ phosphate and the carboxylate substrate. Additionally, Na^+ 3 is located in the monovalent cation-binding site previously identified for D-ala–D-ala ligase, coordinated by the sidechains of Asp301, Asn303, and the backbone carbonyl of Leu303 (15).

Model of L-*Asp and* L-*Met recognition by LdmS*

The stabilization of the closed form by citrate revealed distinct pockets that may accommodate the L-Asp and L-Met substrates (Fig. 6*C*). A polar cavity is formed by the sidechains of Gln244, Tyr252, Asn255, Asn307, and Ser309, and the backbone of Gly308 and Ser309. A hydrophobic cavity is also formed upon closure of the P-loop and N-loop, comprised of Pro26, Leu34, Pro36, Leu44, Tyr111, Ala181, and Tyr184, with the guanidinium sidechain of Arg47 positioned below the cavity opening. Given their nature and relative locations, these sites appeared as candidates for accepting the L-Asp and L-Met sidechains. A narrow solvent accessible channel is also present at the interface of Domains N, B, and C, extending beyond the hydrophobic pocket to an opening formed by Gln40, Phe251, Asn253, Tyr327, Ser328, and His330, indicative of an entry and exit point for substrates and product, respectively (Fig. 6*D*).

Structural comparison of LdmS with characterized LALs revealed the N-loop and the hydrophobic cavity are unique to LdmS (Fig. S5). However, LdmS does contain a region spanning β13 and α12 possessing high structural conservation within the ATP-grasp superfamily, including a Mg^{2+} coordinating acidic residue at the position of Asp301 and the key catalytic residue at the position of Arg305 (Fig. S6). In other

ATP-grasp enzymes, Arg305 plays a key role in recognition of the carboxylate substrate, forming a salt-bridge interaction to position the carboxylate group adjacent to ATP. This aids transfer of the γ phosphate to form the acylphosphate intermediate and also stabilizes the resulting tetrahedral intermediate (26, 27). The conservation of Arg305 in LdmS suggests that the L-Asp substrate is recognized in a similar manner.

To further explore substrate recognition by LdmS, molecular docking was employed. Using the closed form of LdmS as the receptor, L-Asp–L-Met was docked to the region encompassing the polar and hydrophobic cavities. As predicted, the highest scoring pose positioned the L-Asp and L-Met sidechains within the polar and hydrophobic cavities, respectively (Fig. 7*A*). For L-Asp, the β-carboxylate group is positioned toward the Asn255 and Asn307 sidechains and the backbone amides of Gly308 and Ser309, which together present as potential hydrogen bond partners (Fig. 7*B*). This provides an explanation for the preference of L-Asp over L-Asn, with positioning of hydrogen bond donors (NH_2 or NH amides) and acceptors (C=O, O^-) of the interacting residues likely providing selectivity toward L-Asp. This binding mode also explains the inability of LdmS to use bulkier substrates, as they would not be effectively accommodated. The amino group of L-Asp is positioned near the γ phosphate of ATP, suggesting an ionic interaction may be possible. This may account for the inability of LdmS to efficiently utilize L-malate as a substrate, as the 2-OH group would not mediate the same interaction. Additionally, the amide carbonyl is oriented toward Arg305, consistent with Arg305 recognizing the α-carboxylate of L-Asp. The L-Met component of the dipeptide product extends into the hydrophobic cavity and is stabilized by numerous hydrophobic contacts (Fig. 7*C*). Further possible stabilizing interactions are evident for the L-Met carboxylate group, which include a salt bridge with the guanidinium group of Arg47 and a hydrogen bond interaction with the backbone amide of Gly308.

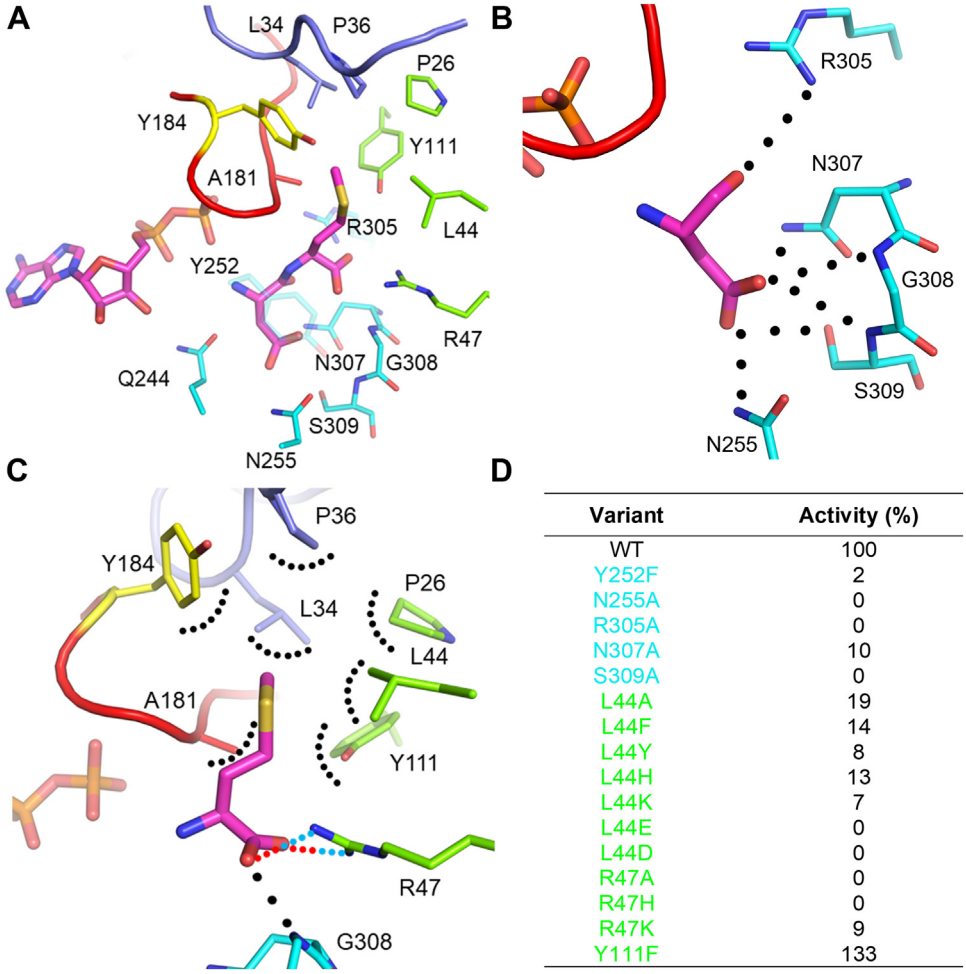

Variant	Activity (%)
WT	100
Y252F	2
N255A	0
R305A	0
N307A	10
S309A	0
L44A	19
L44F	14
L44Y	8
L44H	13
L44K	7
L44E	0
L44D	0
R47A	0
R47H	0
R47K	9
Y111F	133

Figure 7. Investigating substrate recognition by LdmS. *A*, docking model of the L-Asp–L-Met product to LdmS. ADP and the L-Asp–L-Met product are shown as *pink sticks*. *B*, predicted interactions of the L-Asp component within the polar cavity. *C*, predicted interactions of the L-Met component within the hydrophobic cavity. Interacting residues of Domains N and C are shown as *green* or *cyan sticks*, respectively, with Tyr252 shown as transparent sticks for clarity. The P-loop and N-loop are represented by *red* and *purple cartoon*, respectively, with interacting residues shown as *sticks*; for clarity, Tyr184 is shown as *yellow sticks*. The docked L-Asp–L-Met dipeptide and the individual L-Asp and L-Met components are presented as *pink sticks*. Predicted hydrogen bond interactions are indicated by *black circular dashes*, with the predicted salt bridge interaction with Arg47 shown as *red* and *blue circular dashes*. Hydrophobic interactions are indicated by *black circle arcs*. *D*, relative activity of LdmS active site variants for residues forming the polar (*cyan text*) and hydrophobic (*green text*) cavities. Reactions contained 50 mM Tris–HCl pH 8.0, 5 mM $MgCl_2$, 500 μM ATP, 5 mM L-Asp, 5 mM L-Met, and 7.5 nM LdmS variant. LdmS, L-aspartate–L-methionine ligase.

To validate the docking model, mutants of LdmS were generated for residues forming the polar and hydrophobic cavities and the effect on LdmS activity was measured (Fig. 7*D*). Alanine scanning of polar cavity residues predicted to recognize L-Asp supported the docking model. Asn255Ala and Ser309Ala mutants displayed no measurable activity, while an Asn307Ala mutant displayed a 10-fold reduction in activity. This indicates these positions are critical for effective substrate recognition, likely through interaction with the L-Asp β-carboxylate sidechain. Additionally, a Tyr252Phe mutant displayed heavily attenuated activity, suggesting that the hydrogen bond interaction between the OH of Tyr252 and the sidechain amide O of Asn255 is required for stabilizing the respective sidechain groups in a conformation that facilitates L-Asp recognition. An Arg305Ala mutant showed no measurable activity, consistent with the critical role of Arg305 in recognition of the L-Asp α-carboxylate and stabilization of the acylphosphate intermediate and tetrahedral intermediate formed during catalysis.

To probe the role of the hydrophobic cavity in substrate recognition, several mutants with alternate sidechain properties were generated at position Leu44. Substitutions at this site were found to greatly affect LdmS activity. Altering the sidechain to smaller (Leu44Ala) or bulkier (Leu44Phe and Leu44Tyr) groups resulted in attenuated activity. Furthermore, altering the charge of the cavity to be basic (Leu44His and Leu44Lys) or acidic (Leu44Asp and Leu44Glu) greatly reduced or abolished activity. A Tyr111Phe mutant was also generated which possessed comparable activity to WT LdmS, indicating that the OH of Tyr111 is dispensable for substrate recognition. Together, this indicates that the size and hydrophobic nature of this cavity are crucial properties, consistent with this cavity accepting the L-Met substrate. Finally, several mutants were generated at position Arg47. The activity for an Arg47Lys substitution was reduced 10-fold relative to WT LdmS, while Arg47His or Arg47Ala displayed no detectable activity. This supports that Arg47 is directly involved in recognition of the L-Met carboxylate, as the shorter Lys and His sidechains are unable to facilitate this interaction.

The hmrA/ldmS *operon is conserved in* Staphylococcus *and closely related genera*

Having characterized the activity, structure, and mechanism of LdmS, we next sought to gain insight regarding the possible physiological role of the enzyme. To this end, the phylogenetic distribution of LdmS homologs in Prokaryota was investigated as outlined in Experimental procedures. All identified LdmS homologs were exclusive to the Gram-positive phylum Firmicutes (Fig. 8). These were narrowly distributed across several families, including *Staphylococcaceae*, *Caryophanaceae*, and *Thermoactinomycetaceae*. Comparison of the genetic localization for LdmS homologs revealed the *hmrA/ldmS* operon is conserved in all analyzed *Staphylococcaceae*, indicating that LdmS is encoded as part of the core genome in these genera (Fig. S7). The only alteration of the operon architecture was observed for *Abyssicoccus albus*,

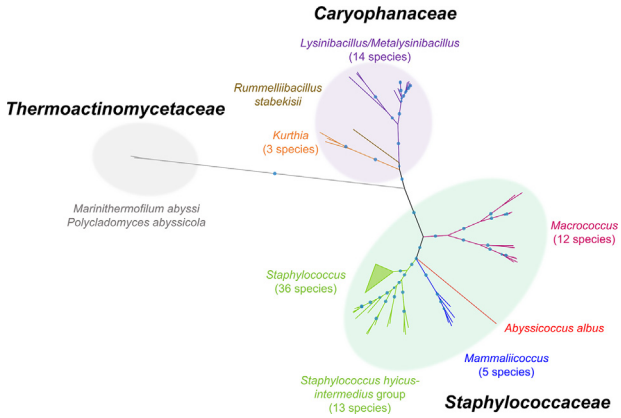

Figure 8. Phylogenetic distribution of LdmS homologs in Prokaryota. Each family is indicated by labels and colored shading, with separate clades color coded and labeled by genus. The genus *Staphylococcus* is split into two branches due to low bootstrap values for the collapsed branch (labeled *Staphylococcus*). Bootstrap values (*blue circles*) for all presented nodes are >0.50. The tree is drawn to scale, with branch lengths measured in the number of substitutions per site. LdmS, L-aspartate–L-methionine ligase.

which possesses an extended *hmrA/ldmS* operon, also encoding a putative Met transporter. In contrast, for *Caryophanaceae*, the *hmrA*/*ldmS* operon was only conserved for *Kurthia* species (Fig. S8). Although the remaining *Caryophanaceae* still possess an HmrA homolog elsewhere in the genome, this indicates that the activities of HmrA and LdmS are likely uncoupled in these genera and suggests LdmS may not facilitate the same functional role as in *Staphylococcaceae*. Finally, for *Marinithermofilum abyssi* and *Polycladomyces abyssicola*, the LdmS homologs were positioned in the vicinity of multiple genes encoding putative ATP-grasp enzymes, suggesting involvement in the step-wise synthesis of an oligopeptide product.

Interestingly, inspection of the 5′ UTR of the *hmrA/ldmS* operon for *Staphylococcus* revealed the presence of predicted *trans*-regulatory elements, the identity of which is species dependent. For *S. aureus*, two motifs are present that match closely to the consensus for the transcriptional regulators CodY and CymR, which both mediate expression of target genes in Gram-positive Prokaryota in response to environmental stress, such as nutrient limitation and oxidative stress (Fig. S9). CodY has been identified to regulate >150 target genes in *S. aureus*, predominantly acting as a transcriptional repressor of genes under nutrient-rich conditions, with DNA binding regulated by Ile and GTP. Under conditions of stress, Ile and GTP are depleted resulting in the upregulation of genes involved in nitrogen metabolism, particularly amino acid biosynthesis and transport, which includes Met biosynthesis and transport (3, 28, 29). CymR similarly acts as a transcriptional repressor by forming a stable complex with the enzyme O-acetylserine sulfhydrylase (CysK) in the absence of oxidative stress, repressing the transcription of target genes involved in Met and Cys metabolism and transport (30). In contrast, for the *Staphylococcus hyicus-intermedius* group, a conserved S-box riboswitch RNA regulatory element was present in the 5′UTR (Fig. S10). Like CodY and CymR, the S-box riboswitch is considered exclusive to Gram-positive Prokaryota, including

Staphylococcaceae, and represses transcription of target genes involved in Met and Cys metabolism under nutrient-rich conditions (14, 31). This is mediated by the essential metabolite SAM, which directly interacts with the S-box to stabilize a terminator helix, resulting in premature termination of transcription. Under conditions of nutrient stress, SAM is depleted, resulting in transcription of target genes. An S-box riboswitch element was similarly observed for the *hmrA/ldmS* operon in *Mammaliicoccus*, *Macrococcus*, and *A. albus*. Combined, these observations strongly support a unique and functionally conserved role for HmrA and LdmS in sulfur amino acid metabolism within these *Staphylococcaceae* genera.

Discussion

The results of the combined biochemical and structural characterization of LdmS provide valuable insight regarding the mechanism behind this novel LAL activity. This supports LdmS adopting a step-wise catalytic mechanism, as per other members of the ATP-grasp superfamily. Additionally, this process appears to be accompanied by restructuring of the active center between two distinct states, supported by the crystallographic capture of LdmS in distinct open and closed states. We propose that apo LdmS initially exists in an open state with the P-loop and N-loop motifs disordered. First, the LdmS–Mg^{2+}·ATP complex forms, resulting in the stabilization and closure of the P-loop. Upon its closure, the P-loop leaves a vacancy into which the N-loop anchors, itself becoming stabilized and adopting a closed conformation. The structural rearrangement of these motifs consequently forms a hydrophobic cavity that accepts the L-Met substrate. This results in the active site being fully enclosed, with the solvent accessible channel at the interface of Domains N, B, and C, the only evident entry point for the L-Asp and L-Met substrates. This indicates that L-Asp is likely to bind first, as L-Met binding would otherwise physically block L-Asp from accessing the polar cavity. Therefore, once this restructuring is complete, we predict that L-Asp enters through the solvent accessible channel and binds to the LdmS–Mg^{2+}·ATP complex (Fig. 9*A*). The L-Asp α-carboxylate group is anchored through forming a salt bridge with Arg305, with the β-carboxylate sidechain stabilized through multiple hydrogen bonds probably involving the sidechains of Asn255, Asn307, Ser309, and backbone amides of Gly308 and Ser309. Once bound, the L-Asp α-carboxylate O^- participates in nucleophilic attack of ATP resulting in the transfer of the γ phosphate of ATP to L-Asp, forming the electrophilic acylphosphate intermediate L-Asp α phosphate (Fig. 9*B*). This is facilitated by the two coordinating Mg^{2+}ions that act as Lewis acids to balance the buildup of negative charge around the phosphoanhydride bond bridging the β and γ phosphates. Once the L-Asp α phosphate intermediate is formed, L-Met then enters through the same channel (Fig. 9*C*).

In order to be utilized, L-Met must be deprotonated. Within the ATP-grasp superfamily, the consensus is that a proton is abstracted from the amino group by an active site base. In LdmS, the obvious candidate is Arg47 as it is the only suitable residue within the vicinity of the active site. Although Arg may generally be considered a poor candidate due to being mostly protonated at physiological pH, several enzymes have been reported to utilize Arg for proton abstraction (32). As Arg47 also appears to directly interact with L-Met, we propose that L-Met is first deprotonated by Arg47, after which the deprotonated form of L-Met binds to LdmS with the sidechain locking into the hydrophobic cavity and the α-carboxylate stabilized through formation of a salt bridge with the now protonated guanidinium group of Arg47. This positions the deprotonated amino group of L-Met adjacent to the L-Asp α phosphate carbonyl to facilitate nucleophilic attack of the carbonyl carbon center to give a phosphorylated tetrahedral intermediate, L-Asp–L-Met α phosphate (Fig. 9*D*). Due to the unstable nature of this tetrahedral intermediate, it has yet to be observed directly in members of the ATP-grasp superfamily. However, cocrystal structures have been captured for numerous ATP-grasp enzymes, including for the LAL BacD, in complex with phosphorylated phosphinate compounds that mimic the tetrahedral intermediate, supporting its formation (27, 33, 34). This intermediate would then collapse to give the final products of ADP, phosphate, and L-Asp–L-Met, with the latter likely diffusing through the solvent accessible channel (Fig. 9, *E* and *F*). Once these products are released, this would destabilize the P-loop and N-loop, returning LdmS to the open form whereby a new catalytic cycle begins.

The characterization of LdmS activity and accompanying genetic analysis performed in this study suggest a role in sulfur amino acid metabolism. As detailed above, the transcriptional regulators CodY and CymR repress the expression of target genes involved in Met and Cys biosynthesis and acquisition in *S. aureus* under nutrient-rich conditions but alleviate this repression under conditions of nutrient stress to increase the intracellular Met and Cys pool. The identification of CodY and CymR consensus elements upstream of the *hmrA/ldmS* operon support that *ldmS* expression is regulated in a similar manner. However, this would make the catalytic activity of LdmS in paradox to these pathways, which would seemingly decrease the pool of intracellular Met through formation of L-Asp–L-Met. To further understand the physiological role and importance of LdmS, future investigation should prioritize (i) the identification and fate of L-Asp–L-Met in *S. aureus*, including the possibility of degradation by HmrA and (ii) the role of LdmS in *S. aureus* pathogenesis and biofilm formation, in both nutrient-rich and nutrient-limited settings. Ultimately, we believe our discovery of LdmS and its future characterization will lead to a more complete understanding of sulfur amino acid metabolism in *S. aureus* allowing for more effective development of new antibiotics that target this pathway.

Experimental procedures

Materials

Oligonucleotides for cloning of LdmS and generation of LdmS variants were purchased from Sigma-Aldrich. Amino acids, amino acid analogs, and nucleoside triphosphates were of ≥90% purity and were obtained from Sigma-Aldrich, except

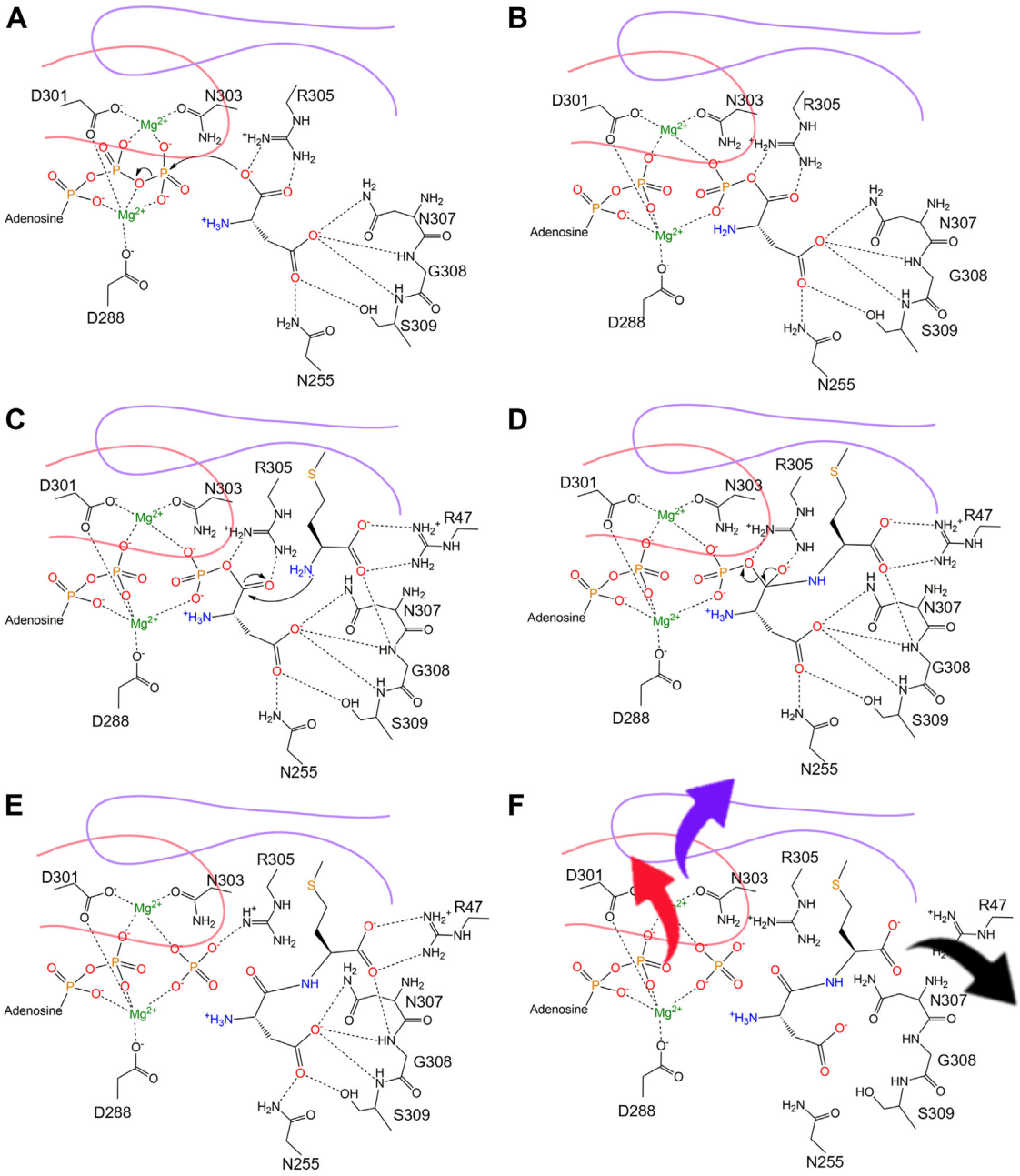

Figure 9. The proposed catalytic mechanism of LdmS. *A–F*, *red* and *purple curves* represent the P-loop and N-loop motifs. Predicted hydrogen bonds and metal coordinating ligands are represented by *dashed lines*. The *curved arrows* in (*F*) represent the dissociation of L-Asp–L-Met (*black*) through the solvent accessible channel and the accompanied destabilization of the P-loop (*red*) and N-loop (*purple*). LdmS, L-aspartate–L-methionine ligase.

for L-Met sulfoxide and N-carbamoyl-DL-Asp which were obtained from Sapphire Bioscience. Aqueous stock solutions of acidic amino acids/amino acid analogs, o-acetyl-L-Ser, L-Tyr, and L-Trp were prepared by adjusting to ∼pH 7 with NaOH. Solutions of labile L-amino acids o-acetyl-L-Ser, L-Cys, and L-homoCys were prepared immediately prior to use. Phosphate standards were prepared from anhydrous potassium phosphate dibasic (KH_2PO_4; >99% purity).

DNA manipulation

For generation of the LdmS expression construct, *saouhsc_02373* was amplified from *S. aureus* NCTC 8325 genomic DNA by PCR, with oligonucleotides incorporating an *N*-terminal poly His-tag and 5′*NdeI* and 3′*BamHI* recognition sites. The resulting fragment was digested with NdeI and BamHI restriction endonucleases, ligated into pMCSG9 and transformed into *E. coli* BL21(DE3) for protein expression. LdmS variants were generated by inverse PCR mutagenesis as previously described, using Phusion high-fidelity DNA polymerase (35). Oligonucleotides used for cloning and mutagenesis are provided in Table S3. The DNA sequence of all LdmS constructs was confirmed by Sanger sequencing.

Expression and purification of LdmS and LdmS variants

Two flasks containing 1 l LB + 100 μg/ml ampicillin were inoculated with 15 ml of a saturated overnight culture and

grown at 37 °C. Upon reaching, an A_{600} of 0.5 expression was induced by the addition of 500 μM IPTG at 16 °C overnight. Cell pellets were collected by centrifugation at 5000*g* (10 min, 4 °C), resuspended in 30 ml total of buffer A (50 mM Tris–HCl pH 8.0, 300 mM NaCl, 10 mM imidazole, 5 mM β-mercaptoethanol) and lysed by mechanical disruption. The lysate was clarified by centrifugation at 40,000*g* (20 min, 4 °C). Clarified lysate was applied to a 5 ml HisTrap HP column (GE Life Sciences) connected to an NGC Medium-Pressure Liquid Chromatography System (Bio-Rad) equilibrated in buffer A, followed by washing with five column volumes of 10% buffer B (50 mM Tris–HCl pH 8.0, 300 mM NaCl, 250 mM imidazole, 5 mM β-mercaptoethanol). LdmS was eluted in a single step with five column volumes of 100% buffer B. Following nickel affinity purification, eluted fractions of WT LdmS were applied to a HiPrep 26/60 Sephacryl S-200 HR gel filtration column (GE Life Sciences) equilibrated with buffer C (20 mM Tris–HCl pH 8.0, 50 mM NaCl, and 1 mM DTT). LdmS was concentrated using an Amicon Ultra centrifugal filter (10,000 molecular weight cutoff, Sigma-Aldrich) to 17 mg/ml and stored at −80 °C. For enzyme activity measurements, LdmS was diluted to 10 μM in buffer C and stored at −80 °C in single use aliquots. LdmS concentration was determined by measuring absorbance at 280 nm using a molar extinction coefficient of 66,240 M^{-1} cm^{-1} and molecular weight of 46,847 Da, as calculated by ProtParam (36).

LdmS variants were expressed in a single 1 l culture and purified by nickel affinity chromatography as described for WT LdmS. For better comparison in activity screening, WT LdmS was also repurified in the same manner. All LdmS variants were then dialyzed against 4 l of buffer C for 16 h at 4 °C. Dialyzed protein was stored at −80 °C in single use aliquots. Concentration of LdmS variants was determined by measuring absorbance at 280 nm using molar extinction coefficients calculated by ProtParam (36). The purity of WT LdmS and all LdmS variants were assessed by SDS-PAGE analysis, revealing high purity (Fig. S11).

Substrate and LdmS variant screening

For screening of LdmS substrate specificity, a colorimetric antimony phosphomolybdate assay was used as previously described, with some modifications (15). All experiments were performed at 37 °C in 96-well half-area microplates (Corning Ref. 3695). Prior to starting the reaction, LdmS and the reaction mixture were equilibrated at 37 °C for 5 min. To start the reaction, 20 μl of 4× LdmS was added to 60 μl of reaction buffer and the sample mixed by pipetting. The reaction was allowed to proceed for exactly 5 min unless otherwise specified. To quench LdmS activity and begin color development, 80 μl of 2× CR (255 mM sulfuric acid, 1.2 mM ammonium molybdate, 18 mM ascorbic acid, and 72 μM potassium antimonyl tartrate) was added to each 80 μl sample and the reactions immediately moved to RT and color developed for 5 min. Color development was quenched with 10 μl of a 30% citric acid solution to prevent interference from acid hydrolysis of ATP, giving a final volume of 170 μl. Absorbance was measured at 850 nm (Pherastar FX microplate reader; BMG Labtech). To account for acid-catalyzed ATP hydrolysis during color development, the absorbance of a no-enzyme blank was subtracted from each sample. For initial probing of LAL activity, all reactions contained 50 mM Tris–HCl pH 8.0, 5 mM $MgCl_2$, and 500 μM ATP. When present, L-Met and "Other aa." were included at a concentration of 2 mM, with LdmS present at a concentration of 50 nM. Reactions were allowed to proceed for 30 min and color developed as detailed above. For identification of L-amino acid substrates and substrate analogs utilized by LdmS, reactions contained 50 mM Tris–HCl pH 8.0, 5 mM $MgCl_2$, 500 μM ATP, and 5 mM of each L-amino acid or analog being assayed. LdmS was initially included at a concentration of 50 nM. As a strong signal was obtained for the L-Met + L-Asp substrate pair, the reaction was repeated with 5 nM LdmS for determination of relative activity. Specific activity was calculated using the slope of a standard curve of KH_2PO_4 in the presence of substrates (Fig. S12). To identify optimal conditions for LdmS activity, initial reaction conditions contained 50 mM Tris–HCl pH 8.0, 5 mM $MgCl_2$, 500 μM ATP, 5 mM L-Asp, 5 mM L-Met, and 5 nM LdmS, with the nucleoside triphosphate (ATP, GTP, CTP, UTP, TTP, or ITP), buffer pH, or divalent metal varied. The result of buffer pH and divalent metal screening are presented in Fig. S6. For screening of LdmS variants, reactions contained 50 mM Tris–HCl pH 8.0, 5 mM $MgCl_2$, 500 μM ATP, 5 mM L-Asp, 5 mM L-Met, and 7.5 nM LdmS variant. All experiments were performed at least twice with duplicate wells for each condition assayed.

Kinetic characterization of LdmS

For determination of WT LdmS kinetic parameters, a pyruvate kinase/lactate dehydrogenase coupled-assay was used as previously described (16). Reactions were performed at 37 °C in 96-well half-area plates (Corning Ref. 3695) in a 100 μl volume containing 50 mM Tris–HCl pH 8.0, 100 mM KCl, 5 mM $MgCl_2$, 1 mM phosphoenolpyruvate, 400 μM NADH, 6 to 10 U ml^{-1} pyruvate kinase, 9 to 14 U·ml^{-1} lactate dehydrogenase, 25 nM LdmS, and varying concentrations of ATP, L-Asp, and L-Met. Prior to starting the reaction, LdmS and the reaction buffer were equilibrated to 37 °C. For determination of K_M values, two of the three substrates ATP, L-Asp, and L-Met were present at fixed concentrations of 2.5 mM, 50 mM, and 10 mM, respectively, being at least 5× the measured K_M value for each substrate. The varied substrate was assayed at seven concentrations ranging between at least 0.2× and 5× the measured K_M. The conversion of NADH to NAD^+ ($\varepsilon_{NADH\cdot340nm}$ = 6220 M^{-1} cm^{-1}) was monitored at 340 nm for 8 min, and the initial velocities determined from linear regression of data collected within the first 3 min of the reaction. To determine kinetic parameters, data were fit with the Michaelis–Menten Equation (Equation 1) by nonlinear regression in GraphPad Prism 6. All experiments were performed 3 times, with duplicate wells for each concentration assayed.

$$v = \frac{v_{max}\,[S]}{K_M + [S]} \quad (1)$$

Characterization of LdmS reaction product by MS

For characterization by MS, a 250 μl sample was prepared containing 50 mM Tris–HCl pH 8.0, 50 mM L-Asp (neutralized to ∼pH 7.5 with ammonia), 50 mM L-Met, 10 mM $MgCl_2$, 25 mM ATP, and 100 nM LdmS. The reaction proceeded at ambient temperature for 24 h, after which reactions were stopped by adjusting to ∼pH 3 through the addition of 2 μl glacial acetic acid. An identical sample containing no LdmS was also prepared by the same method to confirm that observed peaks were a result of LdmS activity. Analysis of reaction products by MS was carried out using an Agilent 6230 time-of-flight instrument coupled to an Agilent 1260 Infinity II LC System. The reaction mixture was diluted 1/100 in 50% aqueous acetonitrile with 0.1% formic acid, and 1 μl was injected and electrosprayed using 50% aqueous acetonitrile with 0.01% formic acid at a flow rate of 0.2 ml/min, without chromatographic separation. ESI-MS conditions were as follows: positive-ion mode; capillary voltage, 3500 V; nozzle voltage 2000 V; fragmentor, 175 V; gas 8 l/min; gas temperature, 325 °C; sheath gas 11 l/min; and sheath gas temperature, 350 °C, *m/z* range, 50 to 1600. MS/MS spectra were acquired on an Agilent 6560 ion mobility quadrupole-time-of-flight instrument coupled to an Agilent 1290 Infinity II LC System. L-Asp–L-Met and L-Met–L-Asp standards were prepared at a concentration of 50 μM in 50% aqueous acetonitrile/0.01% formic acid. These dipeptide standards were synthesized from Boc-L-Met-OH and Boc-L-Asp(OMe)-OH, and Boc-L-Met-OH and L-Asp(OMe)-OMe, respectively, as detailed in Supporting Information Pages 20 to 23. Samples were introduced into the mass spectrometer with ESI-MS conditions as described above, with the following exceptions: nozzle voltage 1000 V; fragmentor, 400 V; targeted mass 281; isolation width 1.3 amu; collision energy 10.

Isolation of LdmS reaction product and characterization by NMR spectroscopy

A 10 ml reaction containing 50 mM Tris–HCl pH 8.0, 20 mM ATP, 5 mM $MgCl_2$, 40 mM L-Asp, 25 mM L-Met, and 100 nM LdmS was incubated at 37 °C for 4 h. Upon completion of the reaction, the sample was stored at −20 °C. Separation of the reaction was performed by semi-preparative RP-HPLC (Gilson GX-Prep) using a Phenomenex Aeris Peptide C18 column (250 × 10 mm). The system was equilibrated with 0.1% TFA in H_2O, with separation achieved using a linear gradient (10–40%) of 0.1% TFA in acetonitrile (20 min, 4 ml·min^{-1}) and visualized at 220 nm and 254 nm. The eluted peak (3.2 min into gradient) was collected and characterized by MS and NMR. Mass spectra were collected on a Bruker HCT Ultra using positive-mode ESI+, connected to an Agilent 1100 LC system running a solvent system of water with 0.1% formic acid and acetonitrile with 0.1% formic acid at 0.1 ml/min. NMR spectra were collected using an Oxford Varian 600 MHz spectrometer and processed in MestReNova v14 or Bruker TopSpin. The sample was dissolved in 10% aq. D_2O ∼pH 4 and referenced to DSS at 0 ppm. A waterES suppression sequence was applied, and zTOCSY and ROESYAD spectra were collected with 256 increments and eight scans. The gHMBCAD spectrum was collected with 256 increments and four scans. Assignment of the isolated product as L-Asp–L-Met is detailed herein:

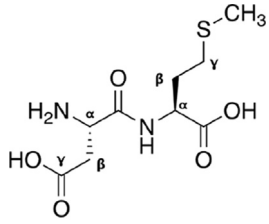

L-Asp–L-Met

The product was isolated from the reaction mixture to give a white powder identified as L-Asp–L-Met. MS (ESI+) expected for $C_9H_{16}N_2O_5S$, 264.3 found 265.30 $(M + H)^+$, 529.70 $(2M + H)^+$. ^1H NMR (599 MHz, 10% aq. D_2O) δ 8.53 (d, J = 7.6, 1H, L-Met NH), 4.58 to 4.50 (m, 1H, L-Met αH), 4.21 to 4.10 (m, 1H, L-Asp αH), 3.08 to 2.95 (m, 2H, L-Asp βH), 2.69 to 2.60 (m, 1H, L-Met γH), 2.60 to 2.49 (m, 1H, L-Met γH), 2.24 to 2.12 (m, 1H, L-Met βH), 2.11 (s, 3H, L-Met CH_3), 2.06 to 1.96 (m, 1H, L-Met βH) ppm. ^{13}C NMR (151 MHz, 10% aq. D_2O) δ 178.5 (L-Met CO), 174.9 (L-Asp γCO), 174.0 (L-Asp CO), 54.7 (L-Met αC), 53.4 (L-Asp αC), 37.2 (L-Asp βC), 32.7 (L-Met γC), 32.0 (L-Met βC), 16.7 (L-Met CH_3) ppm. 2D spectra used for assignment are provided in Fig. S2, *A–D*.

Determination of oligomeric state by native MS

The oligomeric state of LdmS was examined by native MS using a Synapt G1 HDMS (Waters) coupled to a nano-electrospray ionization source. LdmS (1 mg/ml) was buffer exchanged into 200 mM ammonium bicarbonate using an Amicon Ultra-Centrifugal Filter (10,000 MWCO) at 4 °C. Protein was diluted to 0.2 mg/ml and loaded into platinum-coated borosilicate glass capillaries prepared in-house. Key instrument parameters were as follows: capillary voltage (kV): 1.65; sampling cone (V): 50; extraction cone (V): 2.0; trap/transfer collision energy (V/V): 15/10; trap gas (l/h): 5.5; backing gas (mbar): ∼4.5.

Crystallization, data collection, and refinement

LdmS complexes were formed by incubating 17 mg/ml LdmS with 5 mM ATP and 5 mM $MgCl_2$ for 30 min on ice. Crystallization experiments were performed using the sitting drop vapor diffusion method in 96-well Intelliplates (Art Robbins) stored at 16 °C. Conditions promoting crystal formation were probed using the PEG/Ion HT, Index HT, and Crystal Screen HT sparse matrix screens (Hampton Research). Reservoirs contained 80 μl of each condition with drops formed by adding 1 μl of 17 mg/ml LdmS to 1 μl of reservoir solution. Crystals for both the open and closed forms of LdmS were obtained in Crystal Screen HT conditions B10 (200 mM sodium acetate trihydrate, 100 mM Tris–HCl pH 8.5, and 30% PEG 4000) and G4 (1.6 M sodium citrate tribasic dihydrate pH 6.5), respectively.

For data collection, crystals were transferred to Paratone-N for cryoprotection and flash cooled in liquid nitrogen.

Diffraction data were collected at the MX2 beamline of the Australian Synchrotron (37, 38). Indexing, integration, and scaling were completed using XDS, and merging of datasets performed using Aimless (39, 40). Initially, HHPred was used to identify potential models for molecular replacement (41). Top hits were all members of the ATP-grasp superfamily, however, all possessed <20% identity to LdmS. As a result, attempts at solving the phase problem by molecular replacement were unsuccessful. Due to the high resolution diffraction obtained for the open form of LdmS (PDB: 7R8P), *ab initio* methods and fragment-based molecular replacement were explored. Of these, the Fragon pipeline (CCP4i2) successfully solved the phase problem (42, 43). Iterative combinations of one or two ideal helices varying from 5 to 15 amino acids in length were used as the input search model. The combination of two ideal helices of 10 amino acids produced a correlation coefficient (CC_s) of 0.249 after density modification, indicating a successful solution. The resulting model was used as input for AutoBuild (Phenix) to place the remainder of the polypeptide chain and subjected to multiple rounds of rebuilding in Coot followed by refinement in Phenix until the R-factors converged (44, 45). The resulting model was then used to solve the phase problem for the closed form of LdmS (PDB: 7R8Q) by molecular replacement in Phaser, with refinement performed as for the open form (46). For both models, Na^+ ions were identified based on coordinating bond lengths and coordination geometry. All modeled Na^+ possessed octahedral geometry ($^{[6]}Na^+$) with mean bond lengths of 2.45 ± 0.11 Å across both models, consistent with the experimentally determined mean bond length of 2.44 ± 0.11 Å for $^{[6]}Na^+$ bonded to oxygen (47). Data collection, processing, and refinement statistics are presented in Table S4. The final models contained no Ramachandran outliers, with more than 97% of modeled residues favored in the Ramachandran plot. Simulated annealing composite omit maps for the captured ligands of the closed and open forms are provided in Fig. S13.

Molecular docking of L-Asp–L-Met to LdmS

Docking simulations were performed in ICM Pro (Molsoft LLC) using the Small Molecule Docking module which employs a biased probability Monte Carlo procedure (48). The closed form of LdmS complexed with ADP and citrate (PDB: 7R8Q) was used as the receptor, with solvent, metal ions, and citrate removed. The receptor pocket was defined by manual selection of residues forming the polar and hydrophobic cavities (Pro26, Pro36, Leu44, Arg47, Ala181, Gly182, Gly183, Tyr184, Cys225, Gln244, Asn255, Asn307, Gly308, and Ser309). The receptor box was resized to cover this region, defined by two opposing corners with x, y, z coordinates of (14.43, 33.7592, −2.00699) and (24.4342, 48.1948, 8.80468)—a graphical representation is provided in Fig. S14. L-Asp–L-Met was prepared for docking using the ICM-Pro 2D to 3D conversion tool with protonated α-amine group and deprotonated α-carboxylate and β-carboxylate sidechains. Docking was performed with the effort parameter set to 10 and the lowest energy pose used for interpretation.

Identification and phylogenetic analysis of LdmS homologs

For comparative sequence analysis, a protein blast search against the NCBI database was initially performed, identifying >1000 sequences with homology to LdmS. Sequences were filtered to exclude those with <30% sequence identity and <50% sequence coverage. Retained sequences were aligned in MEGA-X using MUSCLE with default parameters. To improve accuracy in assignment of LdmS homologs, only sequences with the key active site residues Arg47, Tyr252, Asn255, Arg305, Asn307, and Ser309 were retained, with sequences containing substitutions at any of these positions removed from further analysis. For the compiled sequences, redundancy was removed through manual curation, with a representative entry retained for each species and the MUSCLE alignment repeated. These aligned representative sequences were used as the input for phylogenetic analysis in MEGA-X through construction of a maximum-likelihood tree using the LG+G+I substitution model with five invariant sites and partial removal of gaps (site coverage cutoff of 95%). The generated tree was tested by the Bootstrap method (200 rounds) and visualized as an unrooted tree using iTOL (49).

Structure comparison and data analysis

Protein secondary structure was assigned using DSSP (50). Sequence-independent structural superposition was performed using The PyMOL Molecular Graphics System Version 2.3.0 (Schrödinger, LLC).

Data availability

Protein crystal structures have been deposited into the RCSB Protein Data Bank with accession codes 7R8P and 7R8Q. The complete phylogenetic tree in Newick format and the MUSCLE alignment used for tree construction are provided for download as Supporting Information 2 and Supporting Information 3, respectively. All remaining data are contained within the article and Supporting Information.

Supporting information—This article contains supporting information (51–64).

Acknowledgments—This research was undertaken in part using the MX2 beamline at the Australian Synchrotron, part of ANSTO, and made use of the Australian Cancer Research Foundation (ACRF) detector. This work was performed in part at the Optofab node of the Australian National Fabrication Facility, a company established under the National Collaborative Research Infrastructure Strategy to provide nano and microfabrication facilities for Australia's researchers. We thank Flinders Analytical (Flinders University) for access and support to IM-MS instrumentation.

Author contributions—J. L. P., A. J. H., B. J., and T. L. P. data curation; J. L. P., A. J. H., B. J., and T. L. P. formal analysis; J. L. P., A. J. H., B. J., and T. L. P. investigation; J. L. P., A. J. H., B. J., and J. K. visualization; J. L. P., A. J. H., B. J., and T. L. P. methodology; J. L. P.

writing–original draft; J. L. P. and J. B. B. project administration; A. D. A., T. L. P., and J. B. B. supervision; J. L. P. and J. B. B. writing–review and editing; J. L. P. conceptualization; A. D. A., T. L. P., and J. B. B. resources.

Conflict of interest—J. L. P. and A. J. H. are recipients of an Australian Government Research Training Program stipend scholarship. The authors declare that they have no conflicts of interest with the contents of this article.

Abbreviations—The abbreviations used are: ESI, electronspray ionization; LAL, L-amino acid ligase; LdmS, L-aspartate–L-methionine ligase; MS, mass spectrometry.

References

1. Kourtis, A. P., Hatfield, K., Baggs, J., Mu, Y., See, I., Epson, E., *et al.* (2019) Vital signs: epidemiology and recent trends in methicillin-resistant and in methicillin-susceptible Staphylococcus aureus bloodstream infections — United States. *MMWR Morb. Mortal. Wkly. Rep.* **68**, 214–219
2. Murray, C. J., Ikuta, K. S., Sharara, F., Swetschinski, L., Aguilar, G. R., Gray, A., *et al.* (2022) Global burden of bacterial antimicrobial resistance in 2019: a systematic analysis. *Lancet* **399**, 629–655
3. Schoenfelder, S. M. K., Marincola, G., Geiger, T., Goerke, C., Wolz, C., and Ziebuhr, W. (2013) Methionine biosynthesis in Staphylococcus aureus is tightly controlled by a hierarchical network involving an initiator tRNA-specific T-box riboswitch. *PLoS Pathog.* **9**, e1003606
4. Krismer, B., Liebeke, M., Janek, D., Nega, M., Rautenberg, M., Hornig, G., *et al.* (2014) Nutrient limitation governs Staphylococcus aureus metabolism and niche adaptation in the human nose. *PLoS Pathog.* **10**, e1003862
5. Jochim, A., Shi, T., Belikova, D., Schwarz, S., Peschel, A., and Heilbronner, S. (2019) Methionine limitation impairs pathogen expansion and biofilm formation capacity. *Appl. Environ. Microbiol.* **85**, e00177-19
6. Annunziato, G., Spadini, C., Franko, N., Storici, P., Demitri, N., Pieroni, M., *et al.* (2021) Investigational studies on a hit compound cyclopropane–carboxylic acid derivative targeting O-acetylserine sulfhydrylase as a colistin adjuvant. *ACS Infect. Dis.* **7**, 281–292
7. Shatalin, K., Nuthanakanti, A., Kaushik, A., Shishov, D., Peselis, A., Shamovsky, I., *et al.* (2021) Inhibitors of bacterial H2S biogenesis targeting antibiotic resistance and tolerance. *Science* **372**, 1169–1175
8. Iyer, L. M., Abhiman, S., Burroughs, A. M., and Aravind, L. (2009) Amidoligases with ATP-grasp, glutamine synthetase-like and acetyltransferase-like domains: synthesis of novel metabolites and peptide modifications of proteins. *Mol. Biosyst.* **5**, 1636–1660
9. Fawaz, M. V., Topper, M. E., and Firestine, S. M. (2011) The ATP-grasp enzymes. *Bioorg. Chem.* **39**, 185–191
10. Chaudhuri, R. R., Allen, A. G., Owen, P. J., Shalom, G., Stone, K., Harrison, M., *et al.* (2009) Comprehensive identification of essential Staphylococcus aureus genes using Transposon-Mediated Differential Hybridisation (TMDH). *BMC Genomics* **10**, 291
11. Santiago, M., Matano, L. M., Moussa, S. H., Gilmore, M. S., Walker, S., and Meredith, T. C. (2015) A new platform for ultra-high density Staphylococcus aureus transposon libraries. *BMC Genomics* **16**, 252
12. Kondo, N., Kuwahara-Arai, K., Kuroda-Murakami, H., Tateda-Suzuki, E., and Hiramatsu, K. (2001) Eagle-type methicillin resistance: new phenotype of high methicillin resistance under mec regulator gene control. *Antimicrob. Agents Chemother.* **45**, 815–824
13. Jamdar, S. N., Are, V. N., Navamani, M., Kumar, S., Nagar, V., and Makde, R. D. (2015) The members of M20D peptidase subfamily from Burkholderia cepacia, Deinococcus radiodurans and Staphylococcus aureus (HmrA) are carboxydipeptidases, primarily specific for Met-X dipeptides. *Arch. Biochem. Biophys.* **587**, 18–30
14. Rodionov, D. A., Vitreschak, A. G., Mironov, A. A., and Gelfand, M. S. (2004) Comparative genomics of the methionine metabolism in gram-positive bacteria: a variety of regulatory systems. *Nucleic Acids Res.* **32**, 3340–3353
15. Pederick, J. L., Thompson, A. P., Bell, S. G., and Bruning, J. B. (2020) D-Alanine–D-alanine ligase as a model for the activation of ATP-grasp enzymes by monovalent cations. *J. Biol. Chem.* **295**, 7894–7904
16. Pederick, J. L., and Bruning, J. B. (2021) An antimony-phosphomolybdate microassay of ATPase activity through the detection of inorganic phosphate. *Anal. Biochem.* **623**, 114170
17. Alreshidi, M. M., Dunstan, R. H., Gottfries, J., Macdonald, M. M., Crompton, M. J., Ang, C.-S., *et al.* (2016) Changes in the cytoplasmic composition of amino acids and proteins observed in Staphylococcus aureus during growth under variable growth conditions representative of the human wound site. *PLoS One* **11**, e0159662
18. Alreshidi, M. M., Dunstan, R. H., Macdonald, M. M., Smith, N. D., Gottfries, J., and Roberts, T. K. (2019) Amino acids and proteomic acclimation of Staphylococcus aureus when incubated in a defined minimal medium supplemented with 5% sodium chloride. *Microbiologyopen* **8**, e00772
19. Murphy, G. R., Dunstan, R. H., Macdonald, M. M., Gottfries, J., and Roberts, T. K. (2018) Alterations in amino acid metabolism during growth by Staphylococcus aureus following exposure to H2O2 – a multifactorial approach. *Heliyon* **4**, e00620
20. Patel, C., Vaishnav, A., Brunzelle, J. S., Guy-Evans, H. I., Edwards, B. F. P., and Evans, D. R. (2018) Targeting aspartate transcarbamoylase in Staphylococcus aureus: a novel therapeutic approach for sepsis. *FASEB J.* **32**, 797.12
21. Gray, B. H., and Bernlohr, R. W. (1969) The regulation of aspartokinase in Bacillus licheniformis. *Biochim. Biophys. Acta Enzymol.* **178**, 248–261
22. Sritharan, V., Wheeler, P. R., and Ratledge, C. (1989) Metabolism of aspartate in Mycobacterium smegmatis. *Eur. J. Biochem.* **180**, 587–593
23. Kobashi, N., Nishiyama, M., and Yamane, H. (2001) Characterization of aspartate kinase III of Bacillus subtilis. *Biosci. Biotechnol. Biochem.* **65**, 1391–1394
24. Jakobsen, Ø. M., Brautaset, T., Degnes, K. F., Heggeset, T. M. B., Balzer, S., Flickinger, M. C., *et al.* (2009) Overexpression of wild-type aspartokinase increases L-lysine production in the thermotolerant methylotrophic bacterium Bacillus methanolicus. *Appl. Environ. Microbiol.* **75**, 652–661
25. Gao, Y., Han, C., Liu, C., Wang, J., Zhao, L., Fang, L., *et al.* (2019) Enzymatic characterization and molecular mechanism of a novel aspartokinase mutant M372I/T379W from *Corynebacterium pekinense*. *RSC Adv.* **9**, 21344–21354
26. Chou, C.-Y., Yu, L. P. C., and Tong, L. (2009) Crystal structure of biotin carboxylase in complex with substrates and implications for its catalytic mechanism. *J. Biol. Chem.* **284**, 11690–11697
27. Shomura, Y., Hinokuchi, E., Ikeda, H., Senoo, A., Takahashi, Y., Saito, J., *et al.* (2012) Structural and enzymatic characterization of BacD, an L-amino acid dipeptide ligase from Bacillus subtilis. *Protein Sci.* **21**, 707–716
28. Pohl, K., Francois, P., Stenz, L., Schlink, F., Geiger, T., Herbert, S., *et al.* (2009) CodY in Staphylococcus aureus: a regulatory link between metabolism and virulence gene expression. *J. Bacteriol.* **191**, 2953–2963
29. Majerczyk, C. D., Dunman, P. M., Luong, T. T., Lee, C. Y., Sadykov, M. R., Somerville, G. A., *et al.* (2010) Direct targets of CodY in Staphylococcus aureus. *J. Bacteriol.* **192**, 2861–2877
30. Soutourina, O., Poupel, O., Coppée, J.-Y., Danchin, A., Msadek, T., and Martin-Verstraete, I. (2009) CymR, the master regulator of cysteine metabolism in Staphylococcus aureus, controls host sulphur source utilization and plays a role in biofilm formation. *Mol. Microbiol.* **73**, 194–211
31. Epshtein, V., Mironov, A. S., and Nudler, E. (2003) The riboswitch-mediated control of sulfur metabolism in bacteria. *Proc. Natl. Acad. Sci. U. S. A.* **100**, 5052–5056
32. Guillén Schlippe, Y. V., and Hedstrom, L. (2005) A twisted base? The role of arginine in enzyme-catalyzed proton abstractions. *Arch. Biochem. Biophys.* **433**, 266–278
33. Fan, C., Moews, P. C., Walsh, C. T., and Knox, J. R. (1994) Vancomycin resistance: structure of D-Alanine:D-Alanine ligase at 2.3 Å resolution. *Science* **266**, 439–443
34. Hiratake, J. (2005) Enzyme inhibitors as chemical tools to study enzyme catalysis: rational design, synthesis, and applications. *Chem. Rec.* **5**, 209–228

35. Fairhead, M., and Howarth, M. (2015) Site-specific biotinylation of purified proteins using BirA. *Methods Mol. Biol.* **1266**, 171–184
36. Gasteiger, E., Hoogland, C., Gattiker, A., Duvaud, S., Wilkins, M. R., Appel, R. D., *et al.* (2005) Protein identification and analysis tools on the ExPASy server. In: Walker, J. M., ed. *The Proteomics Protocols Handbook*, Springer Protocols Handbooks, Humana Press, Totowa, NJ: 571–607
37. Cowieson, N. P., Aragao, D., Clift, M., Ericsson, D. J., Gee, C., Harrop, S. J., *et al.* (2015) MX1: a bending-magnet crystallography beamline serving both chemical and macromolecular crystallography communities at the Australian Synchrotron. *J. Synchrotron. Radiat.* **22**, 187–190
38. Aragão, D., Aishima, J., Cherukuvada, H., Clarken, R., Clift, M., Cowieson, N. P., *et al.* (2018) MX2: a high-flux undulator microfocus beamline serving both the chemical and macromolecular crystallography communities at the Australian Synchrotron. *J. Synchrotron. Radiat.* **25**, 885–891
39. Winn, M. D., Ballard, C. C., Cowtan, K. D., Dodson, E. J., Emsley, P., Evans, P. R., *et al.* (2011) Overview of the CCP4 suite and current developments. *Acta Crystallogr. D Biol. Crystallogr.* **67**, 235–242
40. Kabsch, W. (2010) XDS. *Acta Crystallogr. D Biol. Crystallogr.* **66**, 125–132
41. Zimmermann, L., Stephens, A., Nam, S.-Z., Rau, D., Kübler, J., Lozajic, M., *et al.* (2018) A completely reimplemented MPI bioinformatics toolkit with a new HHpred server at its core. *J. Mol. Biol.* **430**, 2237–2243
42. Jenkins, H. T. (2018) Fragon: rapid high-resolution structure determination from ideal protein fragments. *Acta Crystallogr. D Struct. Biol.* **74**, 205–214
43. Potterton, L., Agirre, J., Ballard, C., Cowtan, K., Dodson, E., Evans, P. R., *et al.* (2018) CCP4i2: the new graphical user interface to the CCP4 program suite. *Acta Crystallogr. D Struct. Biol.* **74**, 68–84
44. Emsley, P., and Cowtan, K. (2004) Coot: model-building tools for molecular graphics. *Acta Crystallogr. D Biol. Crystallogr.* **60**, 2126–2132
45. Adams, P. D., Afonine, P. V., Bunkóczi, G., Chen, V. B., Davis, I. W., Echols, N., *et al.* (2010) PHENIX: a comprehensive Python-based system for macromolecular structure solution. *Acta Crystallogr. D Biol. Crystallogr.* **66**, 213–221
46. McCoy, A. J., Grosse-Kunstleve, R. W., Adams, P. D., Winn, M. D., Storoni, L. C., and Read, R. J. (2007) Phaser crystallographic software. *J. Appl. Crystallogr.* **40**, 658–674
47. Gagné, O. C., and Hawthorne, F. C. (2016) Bond-length distributions for ions bonded to oxygen: alkali and alkaline-earth metals. *Acta Crystallogr. B Struct. Sci. Cryst. Eng. Mater.* **72**, 602–625
48. Abagyan, R., and Totrov, M. (1994) Biased probability Monte Carlo conformational searches and electrostatic calculations for peptides and proteins. *J. Mol. Biol.* **235**, 983–1002
49. Letunic, I., and Bork, P. (2016) Interactive tree of life (iTOL) v3: an online tool for the display and annotation of phylogenetic and other trees. *Nucleic Acids Res.* **44**, W242–W245
50. Kabsch, W., and S, C. (1983) Dictionary of protein secondary structure: pattern recognition of hydrogen-bonded and geometrical features. *Biopolymers* **22**, 2577–2637
51. Tabata, K., Ikeda, H., and Hashimoto, S. (2005) ywfE in Bacillus subtilis codes for a novel enzyme, L-amino acid ligase. *J. Bacteriol.* **187**, 5195–5202
52. Arai, T., Arimura, Y., Ishikura, S., and Kino, K. (2013) L-amino acid ligase from Pseudomonas syringae producing tabtoxin can be used for enzymatic synthesis of various functional peptides. *Appl. Environ. Microbiol.* **79**, 5023–5029
53. Kino, K., Kotanaka, Y., Arai, T., and Yagasaki, M. (2009) A novel L-amino acid ligase from Bacillus subtilis NBRC3134, a microorganism producing peptide-antibiotic rhizocticin. *Biosci. Biotechnol. Biochem.* **73**, 901–907
54. Arai, T., and Kino, K. (2008) A novel L-amino acid ligase is encoded by a gene in the phaseolotoxin biosynthetic gene cluster from Pseudomonas syringae pv. phaseolicola 1448A. *Biosci. Biotechnol. Biochem.* **72**, 3048–3050
55. Noike, M., Matsui, T., Ooya, K., Sasaki, I., Ohtaki, S., Hamano, C., *et al.* (2015) A peptide ligase and the ribosome cooperate to synthesize the peptide pheganomycin. *Nat. Chem. Biol.* **11**, 71–76
56. Kino, K., Noguchi, A., Nakazawa, Y., and Yagasaki, M. (2008) A novel l-amino acid ligase from bacillus licheniformis. *J. Biosci. Bioeng.* **106**, 313–315
57. Kino, K., Nakazawa, Y., and Yagasaki, M. (2008) Dipeptide synthesis by l-amino acid ligase from Ralstonia solanacearum. *Biochem. Biophys. Res. Commun.* **371**, 536–540
58. Senoo, A., Tabata, K., Yonetani, Y., and Yagasaki, M. (2010) Identification of novel L-amino acid alpha-ligases through Hidden Markov Model-based profile analysis. *Biosci. Biotechnol. Biochem.* **74**, 415–418
59. Kino, K., Noguchi, A., Arai, T., and Yagasaki, M. (2010) Identification and characterization of a novel l-amino acid ligase from Photorhabdus luminescens subsp. laumondii TT01. *J. Biosci. Bioeng.* **110**, 39–41
60. Novichkov, P. S., Kazakov, A. E., Ravcheev, D. A., Leyn, S. A., Kovaleva, G. Y., Sutormin, R. A., *et al.* (2013) RegPrecise 3.0 – a resource for genome-scale exploration of transcriptional regulation in bacteria. *BMC Genomics* **14**, 745
61. Database resources of the National Center for Biotechnology Information. *Nucleic Acids Res.* **44**, (2016), D7–D19
62. Doherty, N., Holden, M. T. G., Qazi, S. N., Williams, P., and Winzer, K. (2006) Functional analysis of luxS in Staphylococcus aureus reveals a role in metabolism but not quorum sensing. *J. Bacteriol.* **188**, 2885–2897
63. Mäder, U., Nicolas, P., Depke, M., Pané-Farré, J., Debarbouille, M., van der Kooi-Pol, M. M., *et al.* (2016) Staphylococcus aureus transcriptome architecture: from laboratory to infection-mimicking conditions. *PLoS Genet.* **12**, e1005962
64. Crooks, G. E., Hon, G., Chandonia, J.-M., and Brenner, S. E. (2004) WebLogo: a sequence logo generator. *Genome Res.* **14**, 1188–1190